J Mater Sci: Mater Electron (2012) 23:882–888
DOI 10.1007/s10854-011-0513-8

Effect of synthesis conditions on the preparation of $BiFeO_3$ nanopowders using two different methods

M. M. Rashad

Received: 9 June 2011 / Accepted: 25 August 2011 / Published online: 8 September 2011

Abstract Bismuth orthoferrite ($BiFeO_3$) nanoparticles have been synthesized via the co-precipitation and the oxalate precursor methods. Effects of Bi source, annealing temperature, Bi/Fe molar ratio, oxalic acid ratio and Mn^{2+} ion on the crystal structure, crystallite size, microstructure and magnetic properties of the produced powders were systematically studied. The results revealed that bismuth oxychloride and iron oxide were formed using chlorides sources. A single phase of $BiFeO_3$ was formed from as-made samples with Bi/Fe molar ratio 1.1 using nitrate sources and annealed at 500 and 600 °C for 2 h via the two pathways. The pure $BiFeO_3$ phase appeared as spherical and pseudocubic-like structure using the co-precipitation and the oxalic acid precursor routes, respectively. A high saturation magnetization (3.94 emu/g) was achieved for powder formed from the oxalate precursor route with Bi/Fe molar ratio 1.0 annealed at 600 °C for 2 h as the result of the formation of $Bi_{25}FeO_{39}$. Moreover, Mn^{2+} ion addition affected $BiFeO_3$ properties due to the formation of $Bi_2Fe_2Mn_2O_{10}$. Hence, the saturation magnetization and the coercive force of $BiFeO_3$ were improved substantially by substitution of Mn^{2+} ions ($BiFe_{1-X}Mn_XO_3$, X = 0.1–0.2).

1 Introduction

Bismuth ferrite ($BiFeO_3$) with a perovskite-type structure is extensively studied as a multiferroic material for recent years. $BiFeO_3$ is antiferromagnetic with the Néel temperature $T_N \approx 370$ °C and ferroelectric with the Curie temperature $T_C \approx 830$ °C [1, 2]. These excellent properties make $BiFeO_3$ suitable for applications in radio, television, microwave and satellite communication, bubble memory devices, audio–video, sensors, optical filters, smart devices, high-density ferroelectric random access memory and digital recording fields [3–6]. One of the main obstacles to $BiFeO_3$ applications is a large leakage current because of the existence of the secondary phases such as $Bi_2Fe_4O_9$, $Bi_{25}FeO_{39}$, and $Bi_{36}Fe_{24}O_{57}$ [3]. The traditionally prepared route for $BiFeO_3$ powders is the solid-state reaction of Bi_2O_3 and Fe_2O_3 at a high temperature of 800 °C [7]. At this temperature, pure $BiFeO_3$ is not formed. Nitric acid leaching is required to eliminate the impurity phases such as $Bi_2Fe_4O_9$ and $Bi_{25}FeO_{39}$, after calcination of mixed bismuth and iron oxides in solid state method [7], which resulted in coarse powders and a poor reproducibility. On the other hand, nanosized $BiFeO_3$ material exhibits unique electrical, magnetic and optical properties which are different from the properties of bulk samples due to their low dimensionality and quantum confinement effect. These nanosized-induced properties are expected to widen the potential applications of $BiFeO_3$. To obtain nano-crystalline powders with high homogeneity and uniform structure, many techniques have been provided for the synthesis of the $BiFeO_3$ powders. These methods are co-precipitation [8], hydrothermal [9–14], solvothermal [15, 16], sonochemical [17], microemulsion [17], polyacrylamide gel [18], ferrioxalate [19], sol–gel [6, 20–23], combustion synthesis [7, 24–26], molten-salt [27–29], tartaric acid-assisted gel strategy [30], polymeric precursor [31, 32] and mechanochemical synthesis [33]. The chemical co-precipitation method ensures proper distribution of the various metals ions resulting to stoichiometric and smaller particles size product, compared to some of the other procedures. Moreover, the method is a low-cost

M. M. Rashad (✉)
Central Metallurgical Research and Development Institute,
PO Box 87, Helwan, Cairo, Egypt
e-mail: rashad133@yahoo.com

technique suitable for mass production [34]. In comparison, organic precursor technique involves the chelating of cations in solution by carboxylic acid addition followed by raising the temperature of the solution until the precursor formation. The precursor is consequently annealed at low temperature, which is considered an advantage when compared to other methods. The method is also called a combustion method, a polymeric precursor method, an acid gel method (oxalate precursor, tartaric acid, lactic acid, etc.) and also a Pechini-type process (citrate precursor method). The technique is simple, uses low cost starting materials, low synthesis temperature, yields fine microstructure, homogeneity, narrow particle size distribution and is considered an environmentally friendly methods that offers scalability for large scale production [35, 36]. The properties of $BiFeO_3$ are strongly depending on their chemical composition and microstructure. This, in turn is sensitive on the processing method used. Therefore, in this article, the effect of synthesis conditions on the properties of $BiFeO_3$ nanopowders prepared by two pathways: the co-precipitation and the oxalate precursor methods was systematically studied. Moreover, the effect of Mn^{2+} ion substitution on the crystal structure, microstructure and magnetic properties of $BiFe_{1-X}Mn_XO_3$ particles (with x varying from 0.1 to 0.2) was also investigated.

2 Experimental

The co-precipitation and oxalate precursor methods were applied for the preparation of $BiFeO_3$. Chemically grade anhydrous ferric chloride ($FeCl_3$), ferric nitrate nonohydrate ($Fe(NO_3)_3{\cdot}9H_2O$), bismuth chloride dihydrate ($BiCl_3{\cdot}2H_2O$), bismuth nitrate pentahydrate $Bi(NO_3)_3{\cdot}5H_2O$, manganese nitrate dihydrate ($Mn(NO_3)_2{\cdot}2H_2O$), sodium hydroxide (NaOH) and oxalic acid ($H_2C_2O_4$) were used as starting materials. A series of ferric chloride and/or ferric nitrate (dissolved in distilled water) and bismuth chloride and/or bismuth nitrate solutions with various Bi^{3+}/Fe^{3+}molar ratios from 1.0 to 1.1 was prepared. The orthoferrite precursors were precipitated from these mixtures using 5 M sodium hydroxide solution at room temperature and pH 7. The aqueous suspensions were stirred gently for 15 min to achieve a good homogeneity and to attain a stable pH conditions. The brownish co-precipitates were filtered off, washed with deionized water and dried at 100 °C overnight. For the formation of the $BiFeO_3$ phase, the dry precursors were annealed with a rate of 10 °C/min in static air atmosphere at different temperatures from 500 to 800 °C and then maintained at these temperatures for 2 h. The cooling rate was 20 °C/min. For the synthesis of $BiFeO_3$ by the oxalate precursor route, two mixtures of bismuth/ferric chlorides and bismuth/ferric nitrates solutions were prepared and then stirred for 15 min on a hot-plate magnetic stirrer. Oxalic acid with different molar ratios 1.0 and 1.5 related to Bi^{3+} and Fe^{3+} ions was added gradually into the solution, and then the solution was evaporated at 80 °C with constant stirring to form a viscous resin which dried at 100 °C overnight.

The dried powders obtained as- made samples were annealed with a rate of 10 °C/min in static air atmosphere at the different temperatures from 500 to 800 °C and then maintained at these temperatures for 2 h. To show the effect of substitution of Mn^{2+} ion on the crystal structure, microstructure and magnetic properties, experiments were conducted using two pathways with the substitution of Mn^{2+} ion ($BiFe_{1-X}Mn_XO_3$) where ($x = 0$, 0.1, and 0.2).

The change in the crystal structure was investigated using X-ray powder diffraction (XRD) on a model Bruker axis diffractometer (D8-ADVANCE) with crystallographic data software "Topas 2" with Cu Kα ($\lambda = 1.5406$ Å) radiation, operating at 40 kV and 30 mA with a rate of 2°/min. The diffraction data were recorded for 2θ values between 20° and 80°. Transmission electron microscopy (TEM) images of the formed powders were performed with (TEM, JEOL-JEM-1230 microscope).

The magnetic properties of the products were measured at room temperature using a vibrating sample magnetometer (VSM; 9600-1 LDJ, USA) in a maximum applied field of 15 kOe. From the obtained hysteresis loops, the saturation magnetization (M_s), remanence magnetization (M_r) and coercive field (H_c) were determined.

3 Results and discussion

3.1 Effect of Bi^{3+} ion source

XRD patterns of the as-made samples using $BiCl_3{\cdot}2H_2O$ and $FeCl_3$ as the starting materials with Bi/Fe molar ratio 1.0 and annealed at temperatures from 500 to 800 °C for 2 h using the two pathways are shown in Figs. 1 and 2. It has been shown that BiOCl (JCPDS# 85-0861) was formed as the major phase with the minor impurities Fe_2O_3 (JCPDS# 87-1165) and orthorhombic bismuth pyroferrite $Bi_2Fe_4O_9$ (JCPDS# 72-1832) at annealing temperatures from 500 to 700 °C. Moreover, with increasing the annealing temperature to 800 °C for the co-precipitation method, as shown in Fig. 1, The XRD patterns confirmed the presence of amorphous structure.

Figures 3 and 4 show the XRD patterns of the powders synthesized using bismuth and iron nitrates as the starting materials with Bi/Fe molar ratio 1.0 via the two pathways. The results indicated that a rhombohedral $BiFeO_3$ (JCPDS # 71-2494) was formed as a main phase with the secondary phases of $Bi_2Fe_4O_9$ and Fe_2O_3 using the co-precipitation

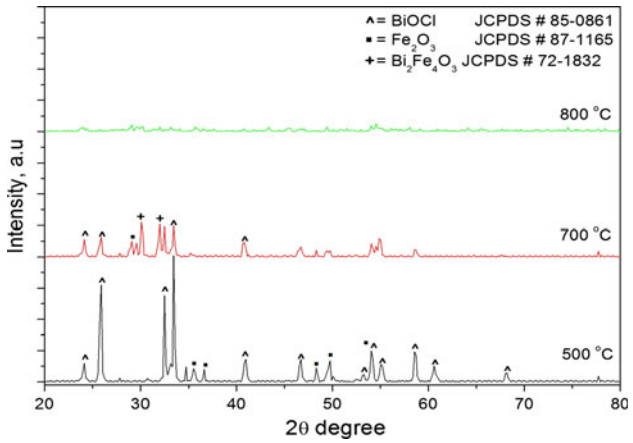

Fig. 1 XRD patterns of the produced powders using chlorides sources precipitated at pH 7 annealed at 500–800 °C for 2 h

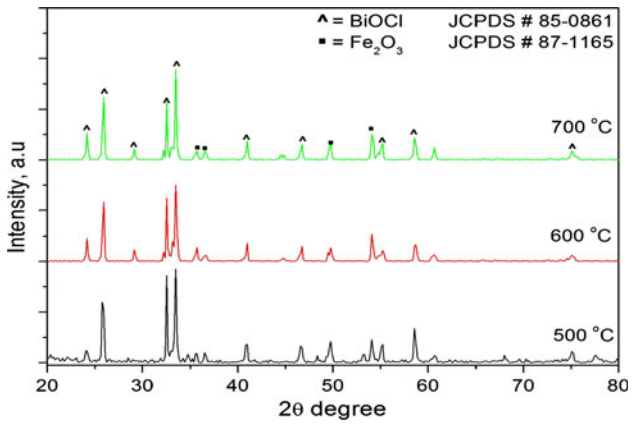

Fig. 2 XRD patterns of the produced powders using chlorides sources with oxalic acid ratio 1 annealed at 500–700 °C for 2 h

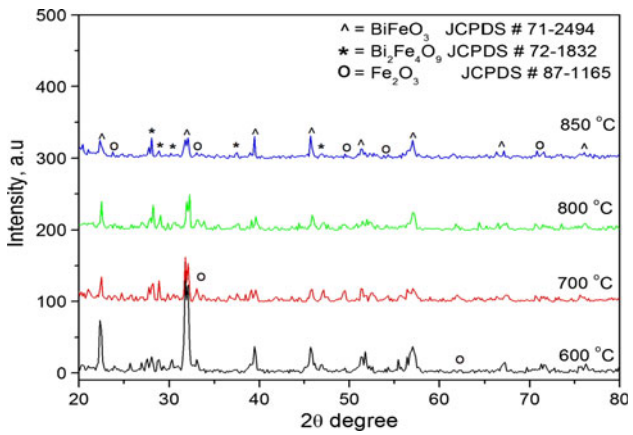

Fig. 3 XRD patterns of the formed powders using nitrates precipitated at pH 7 annealed at 600–850 °C for 2 h

method annealed at different temperatures from 600 to 850 °C for 2 h. The crystallite sizes of the produced $BiFeO_3$ for the most intense peak (1 1 0) plane estimated

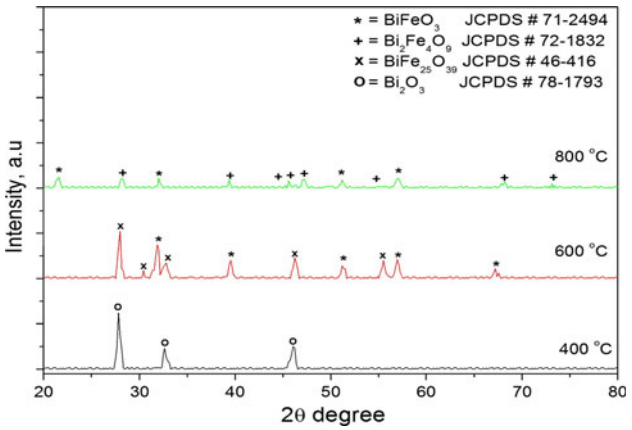

Fig. 4 XRD patterns of produced powders using nitrates sources annealed at 400–800 °C for 2 h using oxalate precursor method

from the X-ray diffraction data using the Debye–Scherrer formula were increased by increasing the annealing temperature. It decreased from 57.3 ± 2 nm at 600 °C to 41.5 ± 2 nm at 700 °C then to 27.7 ± 2 nm at 800 °C, respectively. This could be related to the appearance of secondary phases inside the grain of the $BiFeO_3$ phase (1D growth of nanoclusters of $Bi_2Fe_4O_9$ and $Bi_{25}FeO_{39}$). On the other hand, the powders prepared using the oxalate precursor route is examined by XRD as shown in Fig. 4 and the patterns reflected to the formation of tetragonal bismuth oxide Bi_2O_3 (JCPDS # 78-1793) at low annealing temperature 400 °C. Increasing the annealing temperature to 600, the XRD patterns subjected to form the cubic bismuth iron oxide $Bi_{25}FeO_{39}$ (JCPDS # 46-0416) as the major phase with $Bi_2Fe_4O_9$ and $BiFeO_3$. Further increasing the annealing temperature to 800 °C, $Bi_2Fe_4O_9$ was the major phase with impurities of $BiFeO_3$ and $Bi_{25}FeO_{39}$. The crystallite size of $BiFeO_3$ powders was increased with increasing the annealing temperature. Subsequently, it increased from 21.7 ± 2 at 400 °C to 23.5 ± 2 nm at 600 °C then slightly increased to 24.2 ± 2 nm at annealing temperature 800 °C.

3.2 Effect of Bi/Fe molar ratio

Figure 5 shows the XRD patterns of the samples annealed at 500 and 600 °C for Bi/Fe molar ratio 1.1 using a co-precipitation route. The results revealed that a single rhombohedral $BiFeO_3$ phase with space group R3c was formed at temperatures 500 and 600 °C for 2 h. The crystallinity of the $BiFeO_3$ phase showed a considerably improved with increasing the annealing temperature. Hence, the crystallite size of the produced powders increased rom 32.4 ± 2 nm at 500 °C to 41.7 ± 2 nm at 600 °C. In comparison, XRD patterns of the bismuth iron oxide precursors using Bi/Fe molar ratio 1.1 with oxalic acid molar ratio 1.0 and 1.5

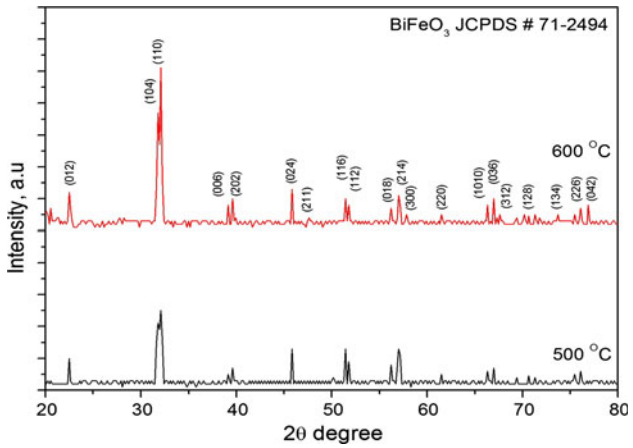

Fig. 5 XRD patterns of $BiFeO_3$ produced at Bi/Fe ratio 1.1 annealed at 500 and 600 °C for 2 h using co-precipitation technique

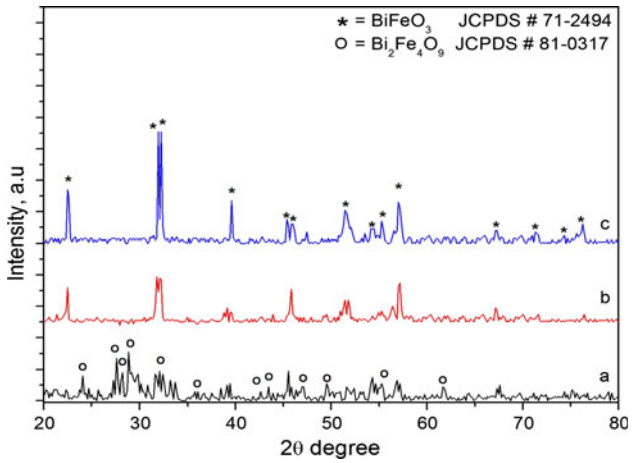

Fig. 6 XRD patterns of $BiFeO_3$ powders produced at Bi/Fe molar ratio 1.1 using oxalate precursor technique *a* excess oxalic acid 1.5 and 500 °C *b* oxalic acid ratio 1 and 500 °C *c* oxalic acid ratio 1 and 600 °C

annealed at 500 and 600 °C for 2 h are given in Fig. 6. It is also evident that the obtained diffraction patterns were corresponded to the standard structure of pure bismuth orthoferrite with the oxalic acid molar ratio 1.0 and annealed at 500 and 600 °C for 2 h. For instance, at the oxalic acid molar ratio 1.5 and the annealing temperature 600 °C, $Bi_2Fe_4O_9$ was formed as the main phase with the $BiFeO_3$. This may be probably attributed to the decomposition of bismuth oxalate with the excess of oxalic acid to bismuth carbonate which reacts with 2 moles of iron oxide according to the following equation:

$$Bi_2(CO_3)_3 + 2Fe_2O_3 \rightarrow Bi_2Fe_4O_9 + 3CO_2 \quad (1)$$

The crystallite size of the produced powders was increased from 29.1 ± 2 at 500 °C to 49.1 ± 2 nm at 600 °C.

TEM micrograph of the pure $BiFeO_3$ obtained by co-precipitation method is displayed in Fig. 7a. The microstructure of the powders appeared as spherical particles which were strongly aggregated as clusters. Furthermore, the particles were more homogeneous and the grains were in narrow size distribution. In contrast, Fig. 7b shows the microstructure of the $BiFeO_3$ particles using the oxalate precursor route appeared as the pseudo-cubic like structure with a relatively uniform grain size distribution.

The magnetization of the produced powders was performed at room temperature under an applied field of 15 kOe and the hysteresis loops of the powders were obtained. Plots of magnetization (M) as a function of applied field (H) for different synthesis conditions are shown in Fig. 8. The results indicated that a slightly increase in the saturation magnetization of the produced samples with the increase the Bi/Fe molar ratio from 1.0 to 1.1 via co-precipitation method. The obtained results agree with the previous published work [1, 37]. The results can be attributed to the $BiFeO_3$ rhombohedral distorted perovskite structure which allows a weak ferromagnetic ordering due to the canting of the spins. The weak ferromagnetic order itself can be understood as a result of noncolinear (canted) spin arrangements in two sublattices [1]. The direction of the small moment equally superimposes a spiral spin arrangement with a crystallite size of

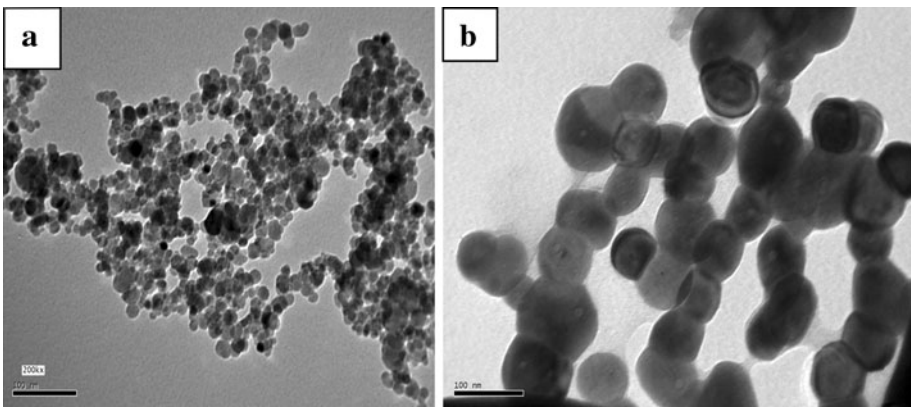

Fig. 7 TEM micrographs of $BiFeO_3$ powders produced at Bi/Fe molar ratio 1.1 annealed at 600 °C for 2 h using **a** co-precipitation **b** oxalate precursor technique

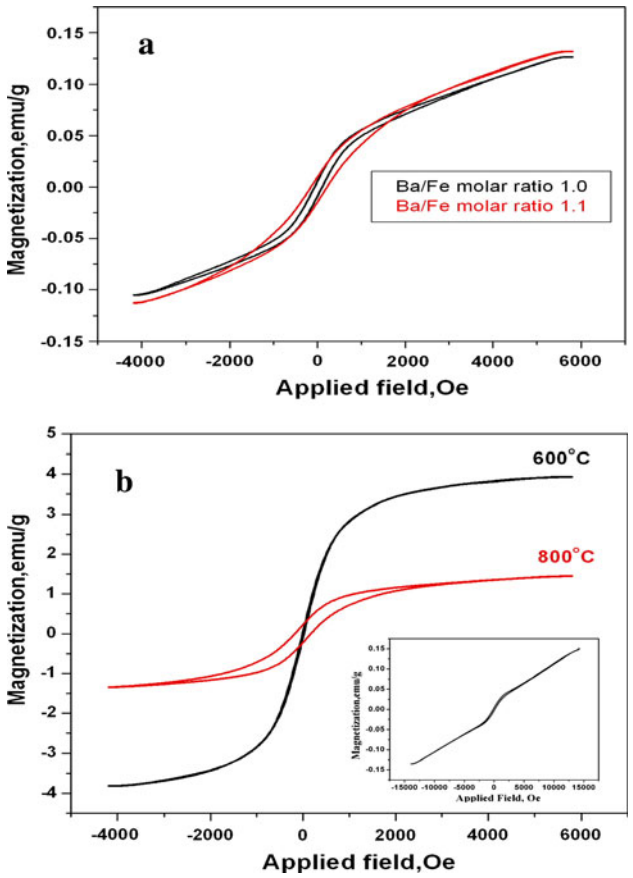

Fig. 8 *M-H* hysteresis loops of the produced powders synthesized using **a** co-precipitation method **b** oxalate precursor route and the intersection is pure $BiFeO_3$ produced at 600 °C

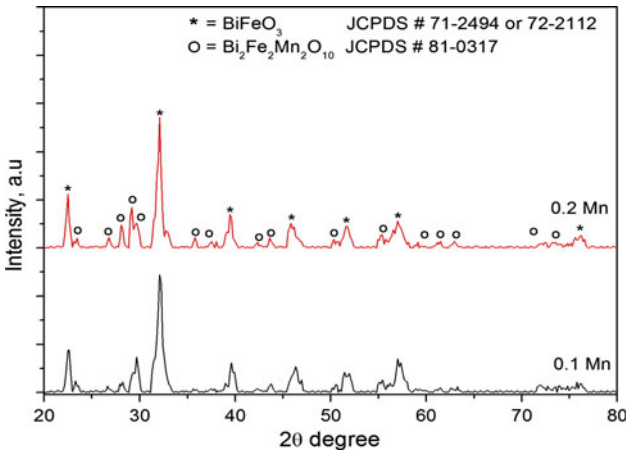

Fig. 9 XRD patterns of the Mn (0.1 and 0.2) doped $BiFeO_3$ powders at Bi/Fe ratio 1.1 annealed at 600 °C for 2 h via co-precipitation technique

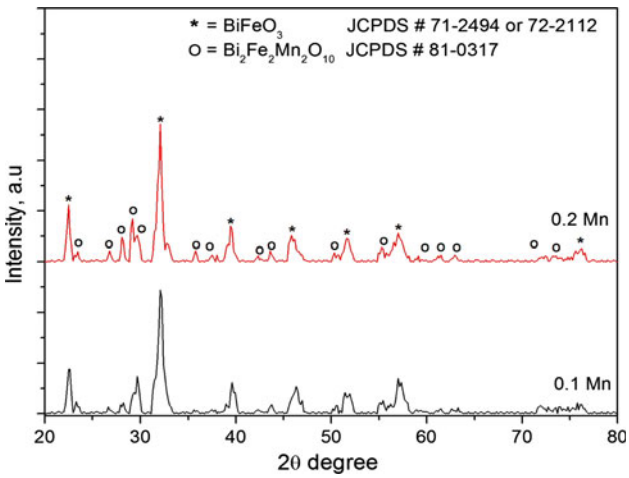

Fig. 10 XRD patterns of the produced Mn doped $BiFeO_3$ powders produced at Bi/Fe molar ratio 1.1 annealed at 600 °C for 2 h using oxalate precursor technique

62 nm, thereby producing a helimagnetic order and a vanishing magnetization in the bulk. Furthermore, $BiFeO_3$ shows a weak ferromagnetic behavior at crystallite size smaller than 62 nm due to the incomplete rotation of the spins along the antiferromagnetic axis [37]. Meanwhile, the coercive field (*Hc*) was increased with increasing the Bi/Fe molar ratio and the annealing temperature. A high coercive field (157.1 Oe) was attributed to the magnetic anisotropy [38]. In comparison, the highest saturation magnetization ($Ms = 3.94$ emu/g) with a low coercive field (20.2 Oe) was achieved for Bi/Fe molar ratio 1.0 annealed at 600 °C for 2 h via the oxalate precursor route due to the formation of $Bi_{25}FeO_{39}$. With further increase of the temperature to 800 °C, the saturation magnetization was decreased to $Ms = 1.42$ emu/g. This value could be related to formation of orthorhombic $Bi_2Fe_4O_9$ as the major phase.

3.3 Effect of Mn^{2+} ion substitution

To explore the effect of manganese substitution and its impact on the properties of the $BiFeO_3$ powders, XRD diffraction patterns of the as- made samples using two pathways with different Mn^{2+} ion molar ratios and annealed at 600 °C for 2 h are given in Figs. 9 and 10. The results revealed that the peaks ascribed to $BiFeO_3$ and $Bi_2Fe_2Mn_2O_{10}$ (JCPDS# 81-317) were observed. The crystallite size of the produced $BiFeO_3$ was decreased with increasing the Mn^{2+} ion ratio. Thereby, it decreased to 22.3 ± 2 and 18.0 ± 2 nm for the co-precipitation route and it decreased to 27.6 ± 2 and 21.8 ± 2 nm with the 0.1 and 0.2 Mn^{2+} molar ratios using the oxalate precursor technique, respectively.

Figure 11 shows the effect of Mn ion ratio on the TEM microstructures of $BiFe_{1-X}Mn_XO_3$ with 0.2 annealed at 600 °C for 2 h. The TEM images of the sample with Mn ions with $x = 0.2$ prepared using the co-precipitation

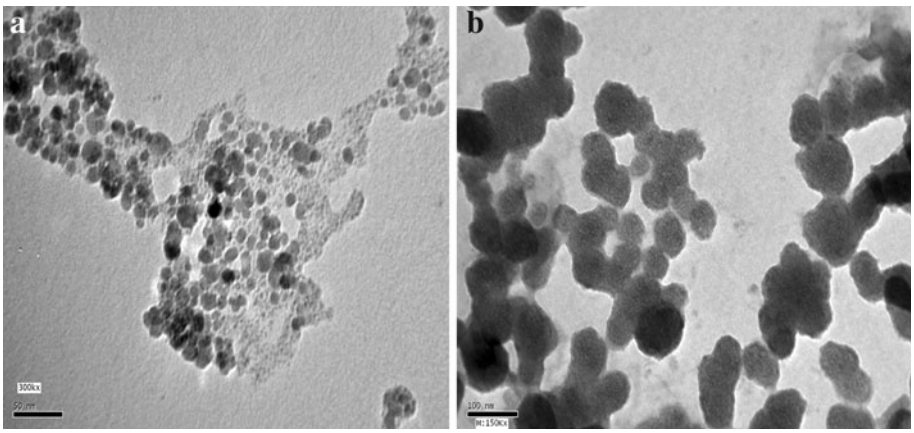

Fig. 11 TEM micrographs of $BiFeO_3$ powders produced at Bi/Fe molar ratio 1.1 annealed at 600 °C for 2 h substituted with 0.2 Mn **a** co-precipitation method **b** oxalate precursor route

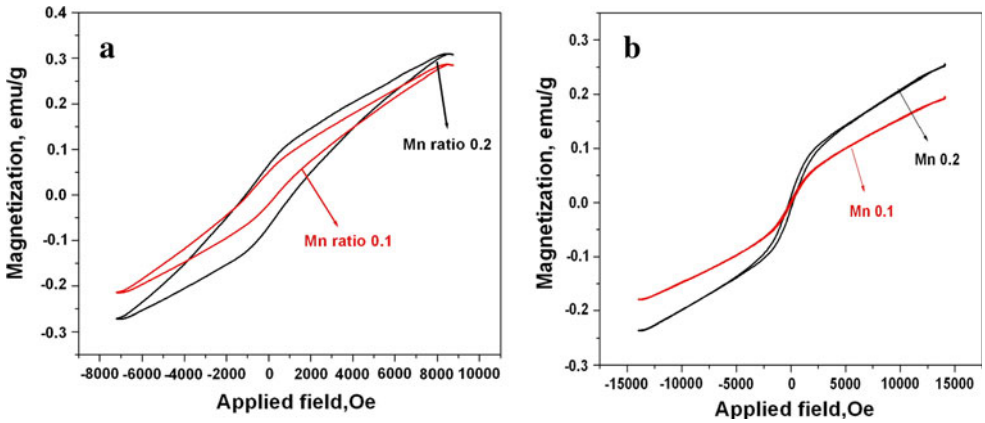

Fig. 12 *M-H* hysteresis loops of the produced Mn doped $BiFeO_3$ powders annealed at 600 °C for 2 h for Bi/Fe molar ratio 1.1 **a** using co-precipitation technique **b** oxalate precursor route

method (Fig. 11a showed microstructure with a discontinuous grain growth with a large unclear crystal structure. In contrast, Fig. 11b shows the microstructure of the powders formed using the oxalate precursor route with Mn^{2+} ion ratio 0.2 appeared as the semi-sphere shapes.

The *M-H* hysteresis loops of the $BiFeO_3$ produced in the presence of 0.1 and 0.2 mol of Mn^{2+} ion annealed at 600 °C with Bi/Fe molar ratio 1.1 using the co-precipitation and the oxalate precursor techniques are given in Fig. 12. The coercivity *Hc* and the saturation magnetization *Ms* of nanoparticles are distinctly influenced by the doping Mn ions. It is seen that *Ms* and *Hc* have greatly improved for both the Mn doped samples due to the formation of $Bi_2Fe_2Mn_2O_{10}$. Due to the similarity of Mn and Fe, which are both 3*d* elements, it is suggested that Mn will substitute Fe. It is reported that B-site ions substitution decreases the magnetic ordering temperature drastically. Due to the intervening of Mn atoms in the Fe atom chains, the antiferromagnetic spin chains of Fe ions are weakened and the ferromagnetic properties are enhanced [39]. The hysteresis loops characteristic of weak ferromagnetism coexists with the non-saturation of the magnetization (Fig. 12a), characteristic of antiferromagnetic ordering of the spins in the nanoparticles. Many researchers have reported that the small particles enhanced magnetization of $BiFeO_3$ which attributed to the surface-induced magnetization, the disappearance of the spiral spin with particles smaller than 64 nm [37] and the ferromagnetism caused by apparent oxygen deficiency [39]. The good saturation magnetization (0.31 emu/g) and the coercive field *Hc* (1135 Oe) were achieved for the powders obtained from the co-precipitated precursor substituted with Mn ion molar ratio 0.2 and Bi/Fe molar ratio 1.1 annealed at 600 °C for 2 h. The values were higher than the *Ms* and *Hc* values of the pure $BiFeO_3$ powders synthesized with the similar conditions without Mn^{2+} addition. The results were related to favorable ferromagnetic properties are achieved when the dimension of $BiFeO_3$ nanoparticles is as small as 30 nm. Moreover, the doping ions can further destroy of spiral modulated spin structure (SMSS). In comparison, Sosnowska et al. [40] have examined the magnetic structures of $BiFe_{1-x}Mn_xO_3$ ($x = 0$, 0.1, and 0.2) polycrystalline samples by a neutron powder diffraction. The results can be explained on the basis of a spiral G-type antiferromagnetic spin structure of undoped—$BiFeO_3$ shifts towards a collinear G-type antiferromagnetic structure with increasing manganese concentration. Such suppression of the spiral spin structure takes place thereby resulting in enhancement of macroscopic magnetization by the canted spin structure. This is presumably responsible for the

enhanced ferromagnetism in Mn doped $BiFeO_3$ nanoparticles [22, 41].

4 Conclusions

The observations from XRD, SEM and VSM studies are summarized as follows:

1. $BiFeO_3$ nanopowders have been synthesized via the co-precipitation and the oxalate precursor routes using nitrates sources as the starting materials
2. The presence of chloride sources in the starting materials led to formation of bismuth oxychloride (BiOCl) and iron oxide (Fe_2O_3)
3. A bismuth surplus was necessary to form pure $BiFeO_3$ phase.
4. The crystallite size was temperature and synthesis routes dependent.
5. The microstructure of the pure $BiFeO_3$ powders appeared as spherical and pseudo-cubic like structure using the co-precipitation and the oxalate precursor routes, respectively.
6. Addition of Mn^{2+} ions affected the crystal structure, crystallite size and the microstructure of $BiFeO_3$ as the result of the formation of $Bi_2Fe_2Mn_2O_{10}$.
7. The highest saturation magnetization (3.94 emu/g) was achieved for the powder formed with Bi/Fe molar ratio 1.0 annealed at 600°C for 2 h due to the formation of $Bi_{25}FeO_{39}$.
8. The saturation magnetization and the coercive field of $BiFeO_3$ were considerably improved by Mn^{2+} ions addition to 0.2.

References

1. C. De Jia, J.-H. Xu, H. Ke, W. Wang, Y. Zhou, J. Euro Ceram. Soc **29**, 3099 (2009)
2. T. Xian, H. Yang, X. Shen, J.L. Jiang, Z.Q. Wei, W.J. Feng, J. Alloys Compd **480**, 889 (2009)
3. S. Farhadi, N. Rashidi, Polyhedron **29**, 2959 (2010)
4. J. Wu, J. Wang, J. Alloys Compd **507**, L4 (2010)
5. J.-H. Xu, H. Ke, C. De Jia, W. Wang, Y. Zhou, J. Alloys Compd. **47**, 2473 (2009)
6. C. Yang, J.-S. Jiang, F.-Z. Qian, D.-M. Jiang, C.-M. Wang, W.-G. Zhang, J. Alloys Compd. **507**, 29 (2010)
7. F.G. Garcia, C.S. Riccardi, A.Z. Simões, J. Alloys Compd. **501**, 25 (2010)
8. S. Ghosh, S. Dasgupta, A. Sen, H.S. Maiti, Mater. Res. Bull. **40**, 2073 (2005)
9. C. Chen, J. Cheng, S. Yu, L. Che, Z. Meng, J. Cryst. Growth **291**, 135 (2006)
10. Y. Wang, G. Xu, L. Yang, Z. Ren, X. Wei, W. Weng, P. Du, G. Shen, G. Han, Ceram. Inter. **35**, 1285 (2009)
11. C.M. Cho, J.H. Noh, I.-S. Cho, J.-S. An, K.S. Hong, J.Y. Kim, J. Am. Ceram. Soc. **91**, 3753 (2008)
12. S.H. Han, K.S. Kim, H.G. Kim, H.-G. Lee, H.-W. Kang, J.S. Kim, C.I. Cheon, Ceram. Inter. **36**, 1365 (2010)
13. Y. Du, Z.X. Cheng, M. Shahbazi, E.W. Collings, S.X. Dou, X.L. Wang, J. Alloys Compd. **490**, 637 (2010)
14. X. Yan, J. Chen, Y. Qi, J. Cheng, Z. Meng, J. Eur. Ceram. Soc. **30**, 265 (2010)
15. A. Chaudhuri, S. Mitra, M. Mandal, K. Mandal, J. Alloys Compd **491**, 703 (2010)
16. Y. Huo, Y. Jin, Y. Zhang, J. Mol. Cat. A: Chem **331**, 15 (2010)
17. N. Das, R. Majumdar, A. Sen, H.S. Maiti, Mater. Lett. **61**, 2100 (2007)
18. T. Xian, H. Yang, X. Shen, J.L. Jiang, Z.Q. Wei, W.J. Feng, J. Alloys Compd **480**, 889 (2009)
19. J. Wei, D.S. Xue, Mater. Res. Bull. **43**, 3368 (2008)
20. J.-H. Xu, H. Ke, C. De Jia, W. Wang, Y. Zhou, J. Alloys Compd. **472**, 473 (2009)
21. D. Huang, H. Deng, P. Yang, J. Chu, Mater. Lett. **64**, 2233 (2010)
22. Z. Wen, X. Shen, D. Wu, Q. Xu, J. Wang, A. Li, Solid State Comm. **150**, 2081 (2010)
23. B.-C. Luo, C.-L. Chen, Z. Xu, Q. Xie, Phy. Lett. A **374**, 4265 (2010)
24. S. Farhadi, M. Zaidi, J. Mol. Catalysis A: Chem. **299**, 18 (2009)
25. M.B. Bellakki, V. Manivannan, C. Madhu, A. Sundaresan, Mater. Chem. Phy. **116**, 599 (2009)
26. A. Hardy, S. Gielis, H. Van den Rul, J. D'Haen, M.K.V. Bael, J. Mullens, J. Euro. Ceram. Soc. **29**, 3007 (2009)
27. X. He, L. Gao, Ceram. Inter. **35**, 975 (2009)
28. T. He, J. Dai, J. Tian, Z. Zhu, L. Guo, Z. Liu, X. Qu, Z. Shen, P. Wang, Ceram. Inter. **34**, 1561 (2008)
29. Y. Yang, J.Y. Sun, K. Zhu, Y.L. Liu, J. Chen, X.R. Xing, Physica B: Cond. Matter **404**, 171 (2009)
30. X. Wang, Y. Zhang, Z. Wu, Mater. Lett. **64**, 486 (2010)
31. M. Popa, D. Crespo, J.M.C. Moreno, J. Am. Ceram. Soc. **90**, 2723 (2007)
32. S.M. Selbach, M.-A. Einarsrud, T. Tybell, T. Grande, J. Am. Ceram. Soc. **90**, 3430 (2007)
33. I. Szafraniak, M. Polomska, B. Hilczer, A. Pietraszko, L. Kepinski, J. Eur. Ceram. Soc. **27**, 4399 (2007)
34. M.M. Rashad, M. Radwan, M.M. Hessien, J. Alloys Compd. **453**, 304 (2008)
35. M.M. Rashad, R.S. Mohammed, A.A. El-Midany, A.T. Kandil, I.A. Ibrahim, J. EurAsian Chem. Technol. **9**, 113 (2007)
36. M.M. Rashad, R.S. Mohammed, M.M. Hessien, I.A. Ibrahim, A.T. Kandil, J. Optoelect. Adv. Mater. **10**, 1026 (2008)
37. X.-Z. Chen, Z.-C. Qiu, J.-P. Zhou, G. Zhu, X.-B. Bian, P. Liu, Mater. Chem. Phys. **126**, 560 (2011)
38. C. Yang, J.-S. Jiang, F.-Z. Qian, D.-M. Jiang, C.-M. Wang, W.-G. Zhang, J. Alloys Compd. **507**, 29 (2010)
39. Q. Xu, H. Zai, D. Wu, Y.K. Tang, M.X. Xu, J. Alloys Compd. **485**, 13 (2009)
40. I. Sosnowska, N.T. Peterlin, E. Steichele, J Phys C: Solid State Phys. **15**, 4835 (1982)
41. X. Yu, X. An, Solid State Comm. **149**, 711 (2009)